Forest Ecology and Management 521 (2022) 120429

Contents lists available at ScienceDirect

Forest Ecology and Management

journal homepage: www.elsevier.com/locate/foreco

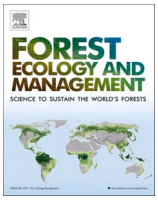

Fire return intervals explain different vegetation cover responses to wildfire restoration in two Sierra Nevada basins

Octavia V. Crompton [a,*], Gabrielle F.S. Boisrame [b], Ekaterina Rakhmatulina [c], Scott L. Stephens [c], Sally E. Thompson [a]

[a] University of Western Australia, Perth, Australia
[b] Desert Research Institute, Las Vegas, NV, United States
[c] University of California, Berkeley, CA, United States

ARTICLE INFO

Keywords:
Fire regime
Forest management
Restoration
Return interval
severity
Exploratory model

ABSTRACT

A simple dynamical model was used to explore the forest cover dynamics for two basins in the Sierra Nevada of California, Illilouette Creek Basin (ICB) in Yosemite National Park and Sugarloaf Creek Basin (SCB) in Sequoia-Kings Canyon National Park. Since the 1970s, fire management in these basins has attempted to restore a near-natural fire regime, after nearly a century of fire exclusion and suppression. The model describes two canopy layers, representing mixed conifer and shrub-dominated landcover types, and is calibrated using landcover maps and fire recurrence and severity data from the ICB. The calibrated model is used to explore several scenarios pertaining to increasing fire severity and return interval in the ICB, and to explore the differences between the ICB and SCB. The results indicate that (i) the ICB in 2012 had not yet reached steady state forest cover, (ii) potential future changes in fire severity and frequency will yield reductions in forest cover, and (iii) differences in forest cover change in response to fire regime restoration between basins can be explained by differences in fire histories.

1. Introduction

Prior to European settlement, California's Sierra Nevada, like many Mediterranean regions worldwide, supported ecosystems and cultures that were ecologically and socially adapted to frequent fire (Taylor et al., 2016; Collins and Stephens, 2007; Taylor and Skinner, 1998). European colonization disrupted these adaptations, preventing cultural burning by Indigenous groups, and suppressing natural, lightning-driven, ignitions (Parsons, 1976; Stephens et al., 2007). For example, the US National Park Service (NPS) in the Sierra Nevada held a fire suppression policy from its founding in 1916 until the late 1960s (Rothman, 2007). Under these policies, fire was almost absent in many areas (other than where infrequent, high-severity wildfires occurred) for nearly 100 years (Collins and Stephens, 2007; Collins et al., 2011; Miller et al., 2012). Removing frequent fire from the landscape may have facilitated forest expansion and shifted forest stands to become more homogeneous and dense (Boisrameé et al., 2022). Ecological changes cascaded as recruitment of fire-adapted vegetation species declined, and the vegetation community composition shifted toward later successional species, with implications for other parts of the ecosystem, for example pollinator diversity (Collins et al., 2011; Collins and Stephens, 2007; Ponisio et al., 2016).

Following the Leopold committee's recommendations that fire be recognized as an ecological process within the US National Parks (Leopold, 1963), the NPS was able to experiment with new fire management approaches. Consequently, in the late 1960s/early 1970s, two remote basins in Yosemite and Sequoia-Kings Canyon National Parks began to burn again. In these basins, naturally occurring fire ignitions were no longer suppressed, and fires were allowed to burn, provided that they did not violate management criteria targeting, for instance, air quality, fire hazards, or protection of sensitive ecosystems (North et al., 2012; Boisramé et al., 2017; Collins and Stephens, 2007). These two basins, Illilouette Creek Basin (ICB) in Yosemite National Park and Sugarloaf Creek Basin (SCB) in Sequoia-Kings Canyon National Park, have now been subject to approximately 50 years of a fire management strategy that approximates a natural fire regime by avoiding suppression of lightning-ignited fires when possible (often referred to as 'managed wildfire'). The multi-decadal duration of managed wildfire policies in

* Corresponding author.
E-mail address: octavia.crompton@duke.edu (O.V. Crompton).

https://doi.org/10.1016/j.foreco.2022.120429
Received 3 September 2021; Received in revised form 9 July 2022; Accepted 15 July 2022
Available online 31 July 2022

Illilouette and Sugarloaf Creek basins provides an invaluable opportunity to learn about the effects of fire on the landscape. Consequently, the basins have been subject to intense research over the past 20 years (Stephens et al., 2021).

Prior to European intervention in the fire regime, most fires in ICB and SCB were thought to be lightning-ignited but Indigenous burning could have occurred. Most fires during the managed wildfire period – initiated in 1969 in SCB and in 1972 in ICB – have been lightning-ignited. Both basins have remained free from logging and roads. We focus on years 1972–2012 for two reasons: firstly, high quality vegetation mapping is available for this period (Boisramé et al., 2017); and secondly, it avoids the extreme 2012–2016 California drought, during which fire suppression was increased to reduce fire risks during abnormally dry conditions. Fire remains relatively less frequent in the basins than it was in the 1700–1900 period, as indicated by fire scar records in trees (Collins and Stephens, 2007). SCB experienced less frequent fire than ICB in all time periods, and a smaller increase in fire frequency in response to the managed wildfire policy. The reasons for this are not fully understood, but may be due to lower forest productivity in SCB, or to the fact that fire suppression has been employed more frequently in SCB during the managed wildfire period than in ICB (Stevens et al., 2020).

The restoration of fire in ICB coincided with large-scale reductions in conifer forest cover, from ~82% cover in 1969 to ~62% cover in 2012, as estimated from forest plot surveys, vegetation mapping and aerial photographic records (Boisramé et al., 2017; Kane et al., 2014). However, similar changes in forest cover did not occur in the SCB, where forest cover remained nearly constant at 83% between 1973 and 2012 (Stevens et al., 2020).

The research undertaken at ICB and SCB over the past 20 years has produced rich datasets that can be used to explore the dynamic interaction of fire and forests. For example, detailed explorations of how fire, land cover change and forest growth have altered the hydrological dynamics of ICB (and the sensitivity of these changes to climate change) have previously been conducted using the process-based ecohydrological model RHESSys (Boisramé et al., 2019; Rakhmatulina et al., 2021). Similar process-based models are available to describe fire ignition and spread (Mann et al., 2016; Coen et al., 2020), as well as forest disturbance and demography (Butler and Dickinson, 2010; Seidl et al., 2011). However, highly resolved process-based models have well-known limitations, including large data requirements to support calibration and validation, computational expense, uncertainty associated with typically high levels of parameterization, and challenges in interpreting cause-and-effect amidst complex interactions between modeled processes. Models of this nature are suitable for making specific quantitative forecasts, and exploring individual scenarios in great detail. An alternative modeling approach is exploratory modeling, which provides an opportunity to relate data and process descriptions to the development and testing of first-order hypotheses (Casagrandi and Rinaldi, 1999; Larsen et al., 2014; Larsen et al., 2016; Rastetter, 2017). In this approach, complex models are replaced by simpler representations of hypothesised underlying processes or dynamics. Such models can usefully synthesize observed phenomena (Wilkening et al., 2021; D'Odorico et al., 2006). They sacrifice process complexity for several benefits: lower computational complexity, clear and even analytical interpretation of the system dynamics and associations between cause and effect, and lower requirements for parameterization, calibration and validation.

A number of important first-order questions about fire-vegetation dynamics in the ICB and SCB, suitable for such exploratory modeling investigations, remain unanswered. In this study, we developed a simple dynamic model describing forest growth in response to fire, and used it to synthesize observations from the basins to address these knowledge gaps. Specifically, we aimed to understand:

1. The long-term response of ICB vegetation cover to the managed wildfire (1972–2012) regime,
2. The implications for the long-term vegetation cover of ICB, if the fire regime were to change relative to the 1972–2012 period, and
3. Why the post-1970 fire regimes in ICB and SCB produced such different vegetation outcomes to date.

The dynamical model we developed draws on elements of several previous simple fire-vegetation models. It follows Casagrandi and Rinaldi (1999) in representing vegetation as an upper and lower canopy, which we interpret as corresponding to forest versus shrub layers. However, we avoid the time-continuous description of fire used by Casagrandi and Rinaldi (1999) and Ursino and Rulli (2011), and instead adopt a stochastic description of discrete fire disturbance events, similar to that used by D'Odorico et al. (2006). The model makes a major spatial simplification in representing the basin as an ensemble of independent point locations, each of which experiences an independent fire history. This means that the model cannot represent the influence of topographic position on fire ignition or severity, and is not suitable for spatial interpretation. Instead, it can be used to predict spatially lumped outcomes such as the basin-wide forest cover fraction, and the proportion of the basin undergoing vegetation cover transitions (forest to shrub or vice versa) in a given period.

The model further simplifies by prescribing fire return intervals and severity. This limits its suitability to represent potential future fire regimes, in which fire severity and frequency will likely be influenced by a number of interacting climatic, vegetation, and human factors (Allen et al., 2015; Abatzoglou et al., 2018). Similarly, the modeling framework does not consider increasing global CO_2 levels, CO_2 fertilization and changing water use efficiency (Hoffmann et al., 2000; Duan et al., 2018; Zhu et al., 2016), or dynamic feedbacks between fire regime and soil/fuel moisture (Miller and Urban, 1999; Rakhmatulina et al., 2021). Thus, long-term drivers of change in forest growth dynamics and fire regimes associated with varying CO_2 concentration and climate are absent from the model. Despite these limitations, the model is amenable to analytical solutions, provided suitable simplifying assumptions are made, allowing for exploration of the system dynamics (e.g., parameter sensitivities).

2. Methods

Casagrandi and Rinaldi (1999) proposed that the growth of seasonally dry, fire-impacted forests could be represented by two coupled differential equations describing the biomass (G, [kg/m^2]) of an upper (u) and lower (l) canopy. The biomass growth of the upper canopy is logistic, and is not affected by the lower canopy biomass. The lower canopy growth is described by a modified logistic model, in which shading from the upper canopy reduces its growth rate via a suppression term proportional to the upper canopy biomass (such that its maximum rate occurs when there is no upper canopy present). We follow Ursino and Rulli (2011) in allowing the growth rate to depend on the soil moisture content within the root zone S [-], which ranges from 0 (no water) to 1 (saturation). The sensitivity of this dependence is controlled by an exponent β, which ranges from 0 (no effect of soil water on growth rates) to 1 (imposing a strong dependence between soil water and growth).

Mathematically, these dynamics are represented by:

$$\frac{dG_u}{dt} = r_u S_u^{\beta} G_u \left(1 - \frac{G_u}{k_u}\right) \tag{1}$$

$$\frac{dG_l}{dt} = r_l S_l^{\beta} G_l \left(1 - \frac{G_l}{k_l}\right) - \alpha G_u G_l, \tag{2}$$

where r is the specific biomass growth rate [1/yr], and α represents the degree of shade inhibition of shrubs by trees [m^2 kg^{-1} yr^{-1}]. k is the

carrying capacity of biomass [kg/m^2], which determines the steady state biomass if fire is removed from the system (the upper canopy biomass G_u approaches k_l, and the lower canopy biomass G_l approaches k_l if shade suppression is also removed).

Fires are stochastically represented as a Poisson process, meaning that the modeled time between two consecutive fires is exponentially distributed (Li et al., 1999; Favier et al., 2004). We specify the exponential rate parameter as $\lambda = 1/RI$, where RI is the return interval (the mean interval between ignitions). In each modeled year, a fire ignition occurs at a given point with probability $p = 1/RI$. If no ignition occurs, the upper and lower canopies continue growing. Fires produced by an ignition event have a random severity (ϕ_u or ϕ_l) which describes the proportional loss of biomass in each canopy layer (i.e. $\Delta G_u = \phi_u G_u$and $\Delta G_l = \phi_l G_l$). The distribution from which fire severities are sampled is described in Section 2.5.2 "Fire severity distribution".

Treating the fire regime as exogenous neglects the influence of topographic position on fire extent and severity (Bradstock et al., 2010; Dillon et al., 2011), which cannot be accommodated in the 1-dimensional modeling framework. During the 1972–2012 calibration period, basin-scale effects of complex topography are implicitly accounted for through model calibration to remotely-sensed fire severity data from the ICB, as described in Section 2.5.2. This approach is reasonable provided that modeled scenarios occur within conditions similar to the calibration period - however, it does not address potential non-stationary relationships between topography and fire severity under climate change (Mackey et al., 2021).

In reality, soil moisture and biomass likely feedback upon both ignition probabilities and severities (Rakhmatulina et al., 2021). Such feedbacks, however, are (i) only one factor among many that influence fire behavior, (ii) difficult to characterize, and likely less important than drivers such as fire weather (Collins et al., 2009; Wayman and Safford, 2021). To avoid imposing an uncertain relationship between fire and vegetation characteristics, we treat all fire parameters (RI and ϕ) as exogenous. Similarly, we assume that soil moisture at a point is independent of the vegetation biomass (which is reasonable for the study sites when considering shrub/forest transitions on annual timescales, see Boisramé et al. (2018)), and we do not address feedbacks between vegetation and hydrological dynamics in the model.

2.1. Analytical stochastic steady state solutions

Analytical solutions for the long-term mean biomass of upper and lower canopies can be obtained subject to the simplifying assumptions that fires occur deterministically every τ years, with a fixed severity ϕ that is identical for the upper and lower canopies. These assumptions fix the biomass density immediately before and after each fire, as illustrated in supporting information Figure S1.

The logistic equation for the upper canopy has the analytic solution:

$$G_u = \frac{k_u G_{uo}}{G_{uo} + (k_u - G_{uo})e^{-r'_u t}} \tag{3}$$

where G_{uo} is the initial biomass (in this case, the biomass immediately after each fire), t is the time in years, and $r'_u = r_u S^\beta$ is an 'effective' growth rate of biomass, which combines the growth rate r_u and growth-limiting factor S^β into a single term.

Integrating Eq. 3 from time $t = 0$ (immediately after a fire) to $t = \tau$ (immediately before the next fire), yields, after simplification, the mean upper canopy biomass density $\widehat{G_u}$:

$$\widehat{G}_u = \frac{k_u}{r'_u \tau} \log\left(1 + \frac{G_{uo}(e^{r'_u \tau} - 1)}{k_u}\right) \tag{4}$$

Eq. 4 describes $\widehat{G_u}$ as a function of the model parameters and the initial biomass density G_{uo}. To determine G_{uo}, the biomass densities at times $t = 0$ and $t = \tau$ can be related using Eq. 3:

$$G_{u\tau} = \frac{k_u G_{uo}}{G_{uo} + (k_u - G_{uo})e^{-r'_u \tau}} \tag{5}$$

By definition, $G_{u\tau}$ and G_{uo} are also related by the fire severity:

$$\phi_u = \frac{\Delta G_u}{G_{u\tau}} = \frac{G_{u\tau} - G_{uo}}{G_{u\tau}}. \tag{6}$$

Rearranging for $G_{u\tau}$:

$$G_{u\tau} = \frac{G_{uo}}{(1 - \phi)} \tag{7}$$

Combining Eqs. 5 and 7 and solving for G_{uo}:

$$\frac{G_{uo}}{(1 - \phi)} = \frac{k_u G_{uo}}{G_{uo} + (k_u - G_{uo})e^{-r'_u \tau}} \tag{8}$$

$$G_{uo} = k_u \frac{1 - \phi - e^{-r'_u \tau}}{1 - e^{-r'_u \tau}} \tag{9}$$

Substituting Eq. 9 into Eq. 4 yields the solution for $\widehat{G_u}$:

$$\widehat{G}_u = k_u \left(1 + \frac{1}{r'_u \tau} \log\left(1 - \phi\right)\right) \tag{10}$$

An approximate analytic solution for the mean biomass density of the lower canopy, $\widehat{G}_l$, may be obtained by replacing G_u with $\widehat{G}_u$ in the lower canopy equation (Eq. 2):

$$\frac{dG_l}{dt} \approx r_l S^\beta G_l \left(1 - \frac{G_l}{k_l}\right) - \alpha \widehat{G}_u G_l, \tag{11}$$

The equation for the lower canopy can then be written in logistic form:

$$\frac{dG_l}{dt} \approx r'_l \left(1 - \frac{G_l}{k'_l}\right) \tag{12}$$

where $r'_l = r_l S^\beta - \alpha \widehat{G}_u$ is a modified growth rate, and $k'_l = k_l r'_l / r_l S^\beta$ is a modified carrying capacity.

Integrating the solution to Eq. 12 (i.e., the solution to the logistic equation, following the same approach as for the upper canopy) yields an approximate solution for the mean lower canopy biomass density, $\widehat{G}_l$:

$$\widehat{G}_l = k'_l \left(1 + \frac{1}{r'_l \tau} \log\left(1 - \phi\right)\right) \tag{13}$$

As detailed in the supporting information Section S1, the errors in this analytical solution compared to numerical simulations were $< 3\%$ when the assumptions of fixed RI and severity were numerically imposed, and $< 9\%$ when ignition was allowed to be random, with fixed severity. While clearly a simplification, the analytic solution enables direct exploration of how the stochastic steady state solutions depend on changing vegetation, fire regime parameters and soil moisture regimes.

2.2. Study Area

Illilouette and Sugarloaf Creek are remote, mid-elevation, conifer-dominated basins located in Yosemite and Sequoia-Kings Canyon National Parks. They are similar in size (ICB: 150 km^2; SCB: 125 km^2) and elevation (ICB: 1800–3000 m; SCB: 2000–3200 m), and have Mediterranean climates featuring winter snow. ICB receives approximately 1000 mm of precipitation annually. There are no long-term in situ weather observations available near SCB, however a variety of indicators point to SCB being drier than ICB (Stevens et al., 2020). Conifer forests in the basins are dominated by *Pinus jeffreyi*, *Abies magnifica*, *Abies concolor* and *P. contorta*. Other common vegetation types include whitethorn ceanothus *Ceanothus cordulatus* shrublands, wet and dry meadows supporting mixed grasses and forbs, and extensive exposed

bedrock (Collins and Stephens, 2007).

2.3. Research studies synthesized

In developing and parameterizing the numerical model for ICB and SCB, we synthesized datasets and findings from nearly two decades of research on the fire, forest and water dynamics of these basins. A full history of the research conducted in the basins is summarized by Stephens et al. (2021). Here, we specifically drew on work from several projects, including vegetation classification and mapping projects (Boisramé et al., 2017; Stevens et al., 2020), soil moisture mapping and prediction efforts (Boisramé et al., 2018; Stevens et al., 2020), and analyses of fire perimeters and severity (Collins et al., 2009; Boisramé et al., 2017; Rakhmatulina et al., 2021), which we briefly summarize next.

Vegetation classification, mapping and landscape ecological analyses for the ICB and SCB (Boisramé et al., 2017**;** Stevens et al., 2020**)**: This work drew on object-oriented classification of aerial photographs of the basins, along with a validated vegetation map of Yosemite National Park produced by the National Park Service. The earliest photos pre-date the first fires occurring under the managed wildfire policies, while later photos coincide with the creation of the Parks Service vegetation map and field visits when vegetation was mapped using handheld GPS units, allowing validation of the classifications used. In the numerical modeling study we use the landcover maps produced for the years 1969 and 2012 from this project. The maps identify regions of sparse meadow (including sparse shrub and/or herbaceous cover), dense meadow (including wetlands and areas of dense herbaceous cover), shrubland, aspen, and mixed conifer forest.

Soil moisture mapping and predictions for ICB and SCB, (Boisramé et al., 2018**;** Stevens et al., 2020**)**: This work used over 6220 individual soil moisture measurements across 90 sites and three years in ICB, to train a random forest model to predict soil moisture using topography, vegetation and fire history at a site. The random forest model was then used to produce maps of summer soil moisture for the basins. Vegetation type was the most important predictor of soil moisture in the basins.

Analyses of fire perimeters and severity for ICB and SCN (Collins et al., 2009**;** Boisramé et al., 2017**;** Rakhmatulina et al., 2021**)**: Fire perimeters were obtained from the Cal Fire, and included all fire extents within Yosemite National Park since 1930. Within each fire perimeter, Landsat observations were used to estimate fire severity, using the RdNDVI (Relative difference Normalized Vegetation Index) and RdNBR (Relative difference Normalized Burn Ratio) indices. RdNBR requires a short-wave infrared band, which is only available after 1984 (Collins et al., 2009); prior to this we approximate RdNBR with RdNDVI. The two indices produce comparable values in ICB and SCB (Rakhmatulina et al., 2021). All RdNBR/RdNDVI values were derived from the Google Earth Engine code described in Parks et al. (2018), using threshold values entered from Miller and Thode (2007). These fire datasets have been used in multiple studies of ICB and SCB including those characterising fire regime, as well as its effects on vegetation, resilience and hydrology.

2.4. Model domain and initialization

We represented the ICB with an ensemble of 400 points sampled from the vegetated portion of the ICB, where sampling excluded the small (< 2%) fraction of the basin supporting dense meadow or aspen (which are not represented in the model). We randomly sampled these locations from a 30 × 30 m vegetation map of ICB and initialized 400 independent model simulations based on the conditions at these sites. To initialize the model, vegetation type was selected for each point from the 1969 landcover map (Boisramé et al., 2017), and used to specify the upper and lower canopy biomass densities, G_u and G_l. For points that were classified as mixed conifer forest in the vegetation map, the upper canopy was initialized at carrying capacity and the lower canopy was initialized at equilibrium with the upper canopy, with $G_l = k_l \cdot (1 - \alpha \cdot k_u / r_l / S^{\beta})$. For points that were classified as shrub or sparse meadow, the lower canopy was initialized at its carrying capacity k_l, and the upper canopy was initialized at 10% of this biomass ($G_u = k_l/10$ kg/m^2), to ensure that some upper canopy biomass is initially present. Shrub and sparse meadow classifications were grouped in this manner because in both cases, the dominant vegetation type is a lower canopy community. Soil moisture maps were previously produced for the same model domain using a random forest model based on extensive soil moisture sampling (Boisramé et al., 2018), and we drew the soil moisture for each pixel from these maps. The distribution of the sampled soil moisture is shown in supporting information Figure S6.

2.5. Model Parameterization

Vegetation and fire severity parameters were obtained from observations in ICB and literature reported values.

2.5.1. Vegetation parameters: growth rates and carrying capacities

The model contains four vegetation growth parameters: two carrying capacities (k_l,k_u) and two growth rates (r_u,r_l). We estimated these values based on previous studies. Gonzalez et al. (2015) measured biomass density in mixed conifer forests in the Sierra Nevada, from which we estimated $k_u = 30$ kg/m^2 (by converting the carbon density of 120 Mg ha^{-1} for mixed conifer forests to kilograms per m^2 and assuming a carbon fraction of 0.47 g carbon (g biomass)$^{-1}$) (Gonzalez et al., 2015).

We estimated the upper canopy growth rate of $r_u = 0.15$ yr^{-1} using the assumptions that sexual maturity for the coniferous forest occurs at 35 years (the median of the dominant conifer species in the basins; Loudermilk et al., 2013; Maxwell and Scheller, 2020), and that conifers reached 80% of the carrying capacity within this time frame. The lower canopy growth rate of $k_l = 6$ kg/m^2 was estimated from reported measurements of the biomass density in *Ceanothus cordulatus* (Huff et al., 2018). We estimated r_l as 1.5 yr^{-1}, assuming that the time to reach sexual maturity in *Ceanothus sp.* is 4 years (Bullock, 1982), and that the biomass densities would be 80% of carrying capacity at this time.

2.5.2. Fire severity distribution

The severity distribution of fires within ICB was estimated using Landsat images of ICB (Boisramé et al., 2017; Collins et al., 2009). The RdNBR data within ICB fire perimeter maps was used to quantify severity in these images using the methods of Miller and Thode (2007), who classified fire severities (unchanged, low, moderate, and high) from remotely sensed RdNBR by comparing them to field observations of the Composite Burn Index. We linearly rescaled the RdNBR observations to severity values ϕ using the bounds of the Miller and Thode (2007) classes, with RdNBR = 316 corresponding to $\phi = 0.5$ and RdNBR = 641 corresponding to $\phi = 0.99$. The resulting distribution of fire severity is shown in Fig. 1. Where RdNBR > 641, we set $\phi = 0.99$, resulting in the bimodal distribution in Fig. 1. This severity distribution was sampled for each ignition event to obtain ϕ_u and ϕ_l values.

2.6. Model Calibration

The remaining model parameters, namely the fire return interval *RI*, the soil moisture sensitivity exponent β, and the competition term α, were set by calibration. The parameters β and α are unknown: we calibrated β over a range of 0–1 (the space on which it is defined), and α over a range of 0–0.06 (outside of which no realistic lower canopy biomass values were obtained). While it would be preferable to avoid calibration of the fire return interval and rely on observational values, the 40 year 1972–2012 period is not long enough to allow a robust estimation of *RI* for use in a stochastic model. We therefore estimated *RI* through calibration, and constrained the estimate using observed rotation periods, defined as the number of years for an area equal to the size of the basin

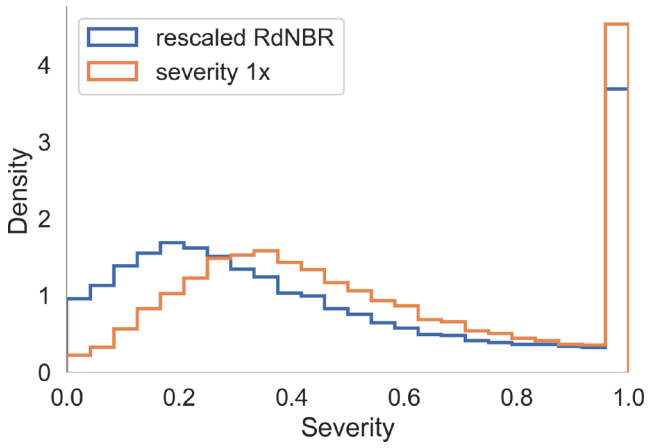

Fig. 1. Fire severity distributions: 'rescaled RdNBR' shows the distribution obtained by rescaling RdNBR data from the ICB, using the severity classes identified in Miller and Thode (2007), and 'severity 1x' shows the increased severity scenario derived by extending the 40 year RdNBR trend for the Sierra Nevada by an additional 20 years (described in Section 2.5.2 "Severi.ty Scenarios"). [See online article for color version of this figure.]

to burn. The fire rotation interval is more appropriate for the 1-dimensional model than the fire return interval, defined as the mean interval between burns *anywhere* in the basin. For the ICB, the rotation intervals were 24.7 and 32.9 years in pre-European and managed wildfire periods, respectively (see Table 1, which summarizes fire frequency characteristics for the basins for the pre-European and managed wildfire periods).

The model performance was assessed in terms of its ability to reproduce four metrics:

1. The change in forest fraction between 1972 and 2012: $\Delta\overline{f}_u(40) = -0.2$.
2. The fraction of the landscape that transitioned from shrub to conifer-dominated between 1972 and 2012, $\overline{f}_{l\to u} = -0.06$ (computed from the vegetation maps).
3. The fraction of the landscape that transitioned from conifer to shrub-dominated between 1972 and 2012, $\overline{f}_{u\to l} = 0.25$ (also computed from the vegetation maps).
4. The difference between the forest cover fraction in 1972 and the model prediction of the forest cover fraction following 100 years of fire suppression, $\Delta\overline{f}_u(100)$.

Evaluating theses metrics requires mapping the simulated biomass fractions, G_l and G_u, to the dominant landcover type - that is, into the binary forest or shrub classes. We treated this classification as simply as possible, setting cases with $G_l > 0.5G_u$ as shrub-dominated, and otherwise as forest-dominated. This is an uncertain choice, but sensitivity analysis revealed minimal changes in the model results when this ratio was set to 0.25 (see supporting information Figure S7). We used this classification to compute the fraction of forest-dominated simulations $\overline{f}_u$ at any point in time, along with the transition metrics $\overline{f}_{l\to u}$ and $\overline{f}_{u\to l}$. Errors in these metrics are reported as the model predictions minus the ICB observations. Thus a positive error in $\Delta\overline{f}_u$ indicates a model bias towards over-predicting forest cover (equivalently, underestimating the decrease in forest fraction during the suppression period).

To test the model against these metrics, we initialized the model with 1972 conditions, following the procedure described in Section 2.4 "Model domain and initialization". The model was initialized for 1144 unique parameter sets, formed by all possible combinations of the parameters listed in Table 2. For each parameter set in the ensemble, 400 independent model simulations were initialized, one for each of the 400 sampled ICB points (for a total of 457,600 simulations). Fig. 2A illustrates an example model run, showing G_u and G_l as functions of time. For a given parameter set i, we computed the forest fraction as a function of time as:

$$\overline{f}_{U,i}\left(t\right) = \frac{1}{n}\sum_{j}^{n=400} x_{u,j}\left(t\right) \tag{14}$$

where $x_{u,j}$ is a binary variable indicating whether simulation j is classified as 'forest' at time t. We similarly computed $\overline{G}_{u,i}$ and $\overline{G}_{l,i}$ as the mean biomass densities across the 400 simulations per parameter set.

The simulations were initialized in the year 1972 and run for 40 years for comparison with the year 2012. The simulations at year 40 were used to test the model performance against the first three test metrics. For each parameter set, the errors associated with metrics 1–3 were obtained from the forest fraction in the year 2012 and the vegetation transitions between 1972 and 2012.

Addressing the fourth test metric required two assumptions. Firstly, we assumed that running the model to steady state under a natural fire regime would approximate the forest conditions prior to fire suppression. For this purpose, the simulations were run for an additional 960 years, at which point in time the forest cover trajectories had reached stochastic steady states. That is, we assumed that simulation year 1000 can approximate forest cover in the year 1872, when fire suppression was imposed. Next, we tested that the 1972 forest cover conditions would be recovered by imposing fire suppression for 100 years on this steady state condition, allowing for comparison of the predicted 'fire suppressed' forest cover and the observed 1972 forest dataset. Subject to these assumptions, we treated the simulation year 1000 as the initial (1872) condition, and ran the model for an additional 100 years with no fire ignitions. We then computed the errors associated with metric 4 as

Table 1
Comparison of fire rotation and return intervals for the ICB and SCB basins in the time periods considered in this study Miller and Thode, 2007. In calibrating the model to ICB, the 1972–2007 period (line 5) was used to estimate the fire rotation period. The return interval is not included for the managed wildfire period for SCB, because only two fires were identified using tree rings in this period, with a 12-year interval between the fires.

Basin	Time period	Fire Rotation Interval (years)	Fire Return Interval (years)
ICB	1700–1900	24.7	6.3
SCB	1700–1900	49.2	9.3
ICB	1900–1972	All fires suppressed	All fires suppressed
SCB	1900–1968	All fires suppressed	All fires suppressed
ICB	1972–2007	32.9	6.8
SCB	1969–2007	79.8	-

Table 2
Model parameters for the calibration simulations. Where multiple parameter values are listed, the simulations were run for factorial combinations of the parameter values.

Variable	Units	Values	Description
Estimated vegetation parameters			
k_u	kg m^{-2}	30	Carrying capacity of the upper canopy
k_l	kg m^{-2}	6	Carrying capacity of the lower canopy
r_u	yr^{-1}	0.15	Specific growth rate of the upper canopy
r_l	yr^{-1}	1.5	Specific growth rate of the lower canopy
Calibration parameters			
α	m^2 kg^{-1} yr^{-1}	0.0, 0.005, 0.01, …0.06	Factor limiting growth of the understory due to competition between species for light
β		0.0, 0.1, … 1.0	Vegetation parameter that quantifies drought tolerance
RI	yr	20, 22, …34	Fire return interval ($1/\lambda$ for random ignition simulations)

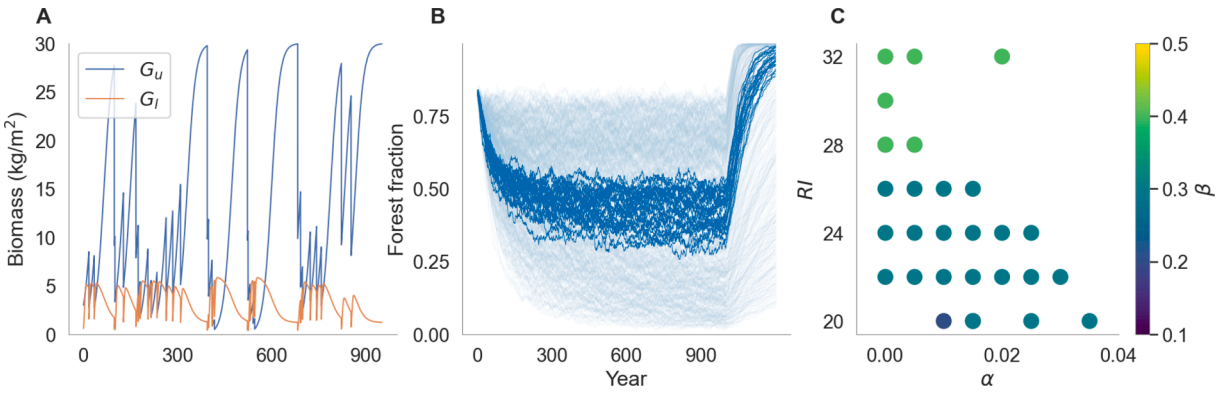

Fig. 2. Panel A shows, for an example simulation, G_u and G_l as a function of time for a single point in space (400 such simulations were averaged per parameter set to compute the forest fraction $\bar{f}_u$ trajectories in Panel B). Panel B shows $\bar{f}_u$ as a function of year, for all tested parameter sets (light blue) and the calibrated parameter sets (dark blue), where fire suppression was implemented in model year 1000. On the right, forest fractions increase above the initial (1972) values under this suppression scenario because the 1972 conditions do not represent steady state conditions (under fire suppressed conditions, the forest fraction approaches 100% in steady state). Panel C shows the distribution of α and *RI* in the calibrated parameter sets, with color indicating β. Note that in this figure, only 27 of the 30 parameter sets can be independently identified, due to overlapping data where different β are associated with the same α and *RI*. [See online article for color version of this figure.]

the difference in forest fraction between simulation years 0 (i.e., using observed 1972 vegetation) and 1100 (which uses the model estimate of what vegetation cover would be in 1972).

2.7. Model prediction

We identified the 30 parameter sets with the lowest errors across all four test metrics. This group, which we refer to as the calibrated parameter ensemble, was used for all subsequent simulations. To use the model for prediction, independent simulations were run for each parameter set in the ensemble (with 400 simulations per parameter set, corresponding to the 400 sampled locations within the basin), producing 30 separate model predictions. The ensemble-mean forest fraction $\langle f_u(t)\rangle$ was then computed as:

$$\left\langle f_u\left(t\right)\right\rangle = \frac{1}{N}\sum_i^N f_{u,i}\left(t\right), \tag{15}$$

where N denotes the 30 parameter sets in the parameter ensemble. Differences in the ensemble forest fraction between time points t_1 and t_0 were computed per parameter set:

$$\left\langle \Delta f_u\left(t_0,t_1\right)\right\rangle = \frac{1}{N}\sum_i^N \left(f_{u,i}(t_1) - f_{u,i}(t_0)\right). \tag{16}$$

Significance was attached to these computations using bootstrapped confidence intervals of the means (i.e., bootstrapping from the results of the 30 selected parameter sets).

2.8. Topic 1: What is the projected long-term response of the ICB vegetation cover to the managed wildfire (1972–2012) regime?

In the absence of temporal trends, a system subject to random disturbance will reach a stochastic steady state, in which the statistics describing the system do not change in time. After 40 years of managed wildfire, analysis of vegetation maps in ICB suggested that this condition was not yet reached (Boisramé et al., 2017). We therefore asked (i) whether the ICB had reached a stochastic steady state after 40 years of managed wildfire, (ii) if not, how 'far' (in terms of mean forest cover) from a stochastic steady state condition the ICB was after 40 years of managed wildfire, and (iii) what the landcover composition of the stochastic steady state condition would be.

We evaluated these questions primarily by comparing the ensemble predictions at times ranging from 40 to 1000 years of simulations. We firstly confirmed that the model predictions were stationary after 1000 years of simulation. We then asked whether predictions at 40, 100, 200, 400, 600, and 800 years were significantly different from the stationary conditions at year 1000, and if so, by how much. This approach re-interprets the simulation year from the calibrated ensemble simulations – instead of interpreting simulation year 1000 as calendar year 1872, we interpret simulation years 40–1000 as calendar years 2012–2972. This approach allows an assessment of whether contemporary (2012) vegetation is approaching stochastic steady state, whether it would be expected to do so within a reasonable policy horizon (100 years), and at what point in time the vegetation dynamics would reach a stochastic steady state.

The aim of these analyses is *not* to forecast future states of the basin: future changes in landcover composition will reflect interactions between vegetation and fire regime, and external forcing such as continuing increases in CO_2 and accompanying changes in hydroclimate. For example, increasing atmospheric CO_2 levels may promote faster growth rates (Donohue et al., 2013), while increased drought frequency or severity may have the opposite effect (Allen et al., 2015). In running the model simulations to steady state, we held the growth rates of the upper and lower canopy layers constant. This means that the long-term model predictions do not account for increasing CO_2 levels, or other drivers of non-stationarity in forest growth behavior and fire regimes that may occur in the coming years. What the analysis provides is an estimate of a response timescale over which the forest would adjust to fire frequency changes, if all other factors were stationary.

2.9. Topic 2: If the fire regime were to change relative to the 1972–2012 period, what would be the implications for the long-term forest fraction of ICB?

We addressed this topic by considering 2 fire regime change scenarios, which altered fire frequency or fire severity independently (described in 2.9.1 anf 2.9.2 and Table 3). For a given scenario, we initialized the calibrated parameter ensemble equivalently to the calibration simulations (i.e., 400 simulations per parameter set). Firstly, the simulations were run for 50 years (to the year 2022), using the observed severity distribution and calibrated return intervals. After 50 years, each scenario was imposed as a step-change in the fire characteristics. We assessed the effects of these imposed regime changes at simulation years 100 (2072) and 600 (by which time simulations were close to steady state). As in Topic 1, these simulations are not intended to forecast future states of the basin, but rather to estimate how forest would adjust

Table 3
Scenarios implemented in ICB and SCB. For the 'ICB potential scenarios', changes in *RI* or severity were applied in 2022, after 50 years of managed wildfire. The RdNBR trend referenced in the severity scenarios is described in Section 3.3 "Severity scenarios".

Scenario	Description
	ICB potential scenarios
RI +30%	30% increase in fire frequency (*RI* values decrease by 30%).
Severity 1x	Sierra Nevada 1982–2018 RdNBR trend continues for 20 years (added 90 RdNBR units to the RdNBR distribution and applied the same transformation to obtain severity).
	SCB test scenarios
RI × 2.4	Calibrated *RI* scaled by a factor of 2.4, based on the observed difference in fire rotation periods.
RI × 2.4, 10% drier	Calibrated *RI* scaled by a factor of 2.4, with soil moisture reduced by 10%

to changes in the current fire regime, all other factors being stationary.

2.9.1. Return interval scenario

Assuming that managed wildfire policies are retained in ICB, climate change may result in increased frequency of ignitions (Westerling and Bryant, 2008; Yue et al., 2014; Westerling, 2018). We followed Westerling and Bryant (2008) and Rakhmatulina et al. (2021) in considering the scenario in which fire frequency increases by 30%. This scenario was implemented for the post-2022 period by reducing the return interval by 30% in each of the calibrated parameter sets.

2.9.2. Severity scenario

In the Sierra Nevada area surrounding ICB, fire severity has increased in recent decades, with RdNBR data for fires in this area from 1983 to 2018 revealing an increase in RdBNR values of 4.5 ± 3.7 year^{-1} (Rakhmatulina et al., 2021). However, over the managed wildfire period, ICB itself has not experienced a trend in fire severity (Rakhmatulina et al., 2021), making it challenging to predict future changes in fire severity. We therefore elected to explore the model sensitivity to fire severity by projecting the 1983–2018 Sierra Nevada trend 20 years into the future, resulting in a 90 unit increase in RdBNR (the 'severity 1x' scenario). To apply these projections as step changes, we uniformly shifted the RdNBR data for ICB by 90 or 180 units, and then rescaling to severity ϕ as per Section 2.5.2 "Fire severity distribution". These transformations (see Fig. 1) result in an increase of the mean ϕ from 0.45 (observed) to 0.54 (severity 1x).

2.10. Topic 3: Why did the post-1970 fire regimes in ICB and SCB produce such different vegetation outcomes to date?

A number of hypotheses have been proposed to explain the differences between the ICB and SCB responses to fire management. The simplest of these include the greater fire frequency observed in ICB compared to SCB, while more complex hypotheses postulate that stand-replacing fire was more frequent in ICB than SCB, potentially due to differences in overall climate, soil and basin productivity, and fire management interventions themselves (Stevens et al., 2020; Stephens et al., 2020). Although we cannot use the simple model presented here to assess underlying feedbacks between vegetation and fire regime, we can use it to ask whether similar basins exposed to different fire frequencies over the managed wildfire period would produce the observed divergent outcomes, all other factors being equivalent, or whether additional changes (e.g. to forest growth rates) need to be included for the models to reproduce the minimal changes observed in SCB. We followed this strategy in part because there is not enough data to independently calibrate the model for SCB. Thus, the SCB simulations use the ICB calibrated parameter ensemble for α or β. Given the similarity in land-cover and climate between basins, this is a reasonable assumption (Collins et al., 2016). SCB and IBC had similar forest cover fractions when fire suppression was reversed, so SCB simulations were initialized in the same way as ICB.

We then considered several scenarios. Firstly, we held all drivers common between SCB and ICB, other than fire frequency, which was adjusted to match ICB. To perform this adjustment, we scaled the return intervals in the calibrated parameter set by a factor of 2.4, which is the approximate ratio of the rotation periods between basins during the managed wildfire period (Collins and Stephens, 2007).

Next, we considered altering the severity distributions; however, for the managed wildfire period, the estimated proportion of area burned at high severity was comparable between the basins (based on Landsat-derived RdNBR data; (Parks et al., 2018)).

Finally, we considered the various lines of evidence that point to SCB being drier than ICB (Stevens et al., 2020), and how this, in addition to a longer fire return interval, could affect forest cover changes. While field measurements and associated models suggest higher mean soil moisture in ICB compared to SCB (Stevens et al., 2020; Boisramé et al., 2018), there is insufficient data to directly evaluate differences in the average water availability between the basins. Instead, we used the normalized difference vegetation index (NDVI) as a proxy for productivity and thus soil moisture. We rescaled the soil moisture in ICB pixels by the ratio of NDVI between the basins (NDVI in ICB was approximately 10% greater than in SCB for the 1984–1985 period; (Stevens et al., 2020)) and repeated the fire frequency simulations.

For all modeled scenarios, we compared the 1972 forest fraction to model predictions after 40 years of managed wildfire policy.

2.11. Analytical predictions

To provide context for the forest-fire dynamics predicted by the numerically modeled scenarios, we applied the analytical solution to the ICB using the calibrated parameters. Making direct comparisons between modeled and analytical results required (i) replacing the distribution of sampled severities with a single 'effective' fire severity, and (ii) obtaining an estimate of the forest cover fraction $\widehat{f}_u$ from analytical predictions of upper and lower canopy biomass. To estimate the effective fire severity, we inverted Eq. 10 for $\widehat{G}_u$ to obtain an effective upper canopy severity, $\widehat{\phi}_u$:

$$\widehat{\phi}_u = 1 - \exp\left(r_u' RI \left(\frac{\widehat{G}_u}{k_u} - 1 \right) \right) \tag{17}$$

yielding a unique value of $\widehat{\phi}_u$ for each of the 30 calibrated parameter sets (i.e., for each RI, β and α combination), using the mean S value for all sampled pixels. We repeated this process for the lower canopy and checked for agreement between the effective severities (see supporting information Figure A). To estimate the forest fraction from predicted $\widehat{G}_l$ and $\widehat{G}_u$, we fit a random forest model to all data from the numerical simulations, predicting $\overline{f}_u$ as a function of the ratio of $\overline{G}_l/\overline{G}_u$, α and β. This was needed because the analytic model predicts $\widehat{G}_l$ and $\widehat{G}_u$, but not $\widehat{f}_u$; thus, model fit to the numerical simulations was used to relate these quantities. The model performed very well, with a test set score of $R^2 > 0.99$ using cross validation. Analytical solutions were therefore presented in terms of the direct analytical solutions for $\widehat{G}_u$, and $\widehat{G}_l$, and the estimated $\widehat{f}_u$ associated with them.

3. Results

3.1. Calibration

Selection of the 30 parameter sets with the lowest errors produced calibration errors less than 5.7% across all four test metrics (see supporting information Figure S8 showing histograms of the calibration errors). The forest fraction trajectories predicted from the calibrated

parameter sets (dark blue lines in Fig. 2B) reproduce the 20% decrease in ICB forest fraction between 1972 and 2012 and recover the initial (1972) conditions following 100 years of fire suppression (simulation years 1000–1100 corresponding to calendar years 1872–1972).

Associations between *RI* and β in the calibrated parameter set (see Fig. 2C) reflect opposing influences of these parameters on the system dynamics. Increasing *RI* favors higher G_u, because the slower-growing upper canopy benefits from longer periods of recovery. By contrast, increasing β, which reduces the drought tolerance, suppresses the growth rates of both canopies; however, in the case of the lower canopy, the benefits of suppressing the upper canopy outweigh the costs of reduced drought tolerance. Smaller return intervals are similarly associated with larger α in the calibrated parameter set, because increasing α suppresses lower canopy growth, which compensates for the faster lower canopy growth rates. Thus, compensating effects of the parameters with respect to G_u and G_l (and thus the forest fraction), result in correlation within the calibrated parameters. In spite of these compensating effects, small errors across all four test metrics suggest that the parameters have been well identified (see supporting information Table S2, which lists the calibrated parameters – α, β and *RI* values – along with the errors in the calibration metrics).

3.2. Steady state

To confirm that the vegetation trajectories reached a steady state within 1000 years of simulation, we compared the forest fraction in the final century of managed wildfire policy to the prior century (i.e., between simulation years 900–1000 and 800–900). The $\bar{f}_u$ distributions are not significantly different between these periods, in either the calibrated parameter ensemble or the ensemble of tested parameters (using the Kruskal–Wallis H-test).

Summarizing the ensemble simulations, the results suggest that the vegetation in ICB was not in steady state in 2012. The ensemble predictions of the forest fraction between 40 and 1000 years did not overlap (Fig. 3A), and the ensemble average difference between timesteps did not cross zero (Fig. 3B). The predicted stochastic steady state forest fraction was $\langle f_u \rangle = 0.43 \pm 0.02$ (Table 4), with approximately 100 years (from 1972) required for the ICB forest cover dynamics to approach within 10% of these steady state conditions. In 2012, the basin forest cover was approximately half-way between its fire-suppressed initial and a stochastic steady state condition in dynamic equilibrium with the (current) managed wildfire regime. (See Table 5).

Table 4
Ensemble predictions of ICB forest cover (calibration parameter sets only) over multiple simulation durations. The section 'Ensemble prediction of $\langle f_u \rangle$' shows the ensemble prediction of the forest fraction f_u, with bootstrapped confidence intervals in parentheses, for select simulation years ranging from 40 to 1000. Rows labeled 'Difference from $t = 40$ years' show the ensemble average difference between 2012 (simulation year 40) and two subsequent timesteps (simulation years 100 and 1000). The final section, labeled 'Difference from $t = 1000$ years' shows the ensemble average difference between the year 1000 and previous timesteps. The results suggest that the ensemble is in steady state by the year 600; however, the difference between the years 200 and 1000 is already small ($\langle \Delta f_u \rangle = -0.05 \pm 0.02$).

Simulation year	$\langle f_u \rangle$
Ensemble prediction of $\langle f_u \rangle$	
0	0.83 (0.83, 0.83)
40	0.65 (0.64, 0.66)
100	0.54 (0.53, 0.55)
200	0.48 (0.47, 0.50)
400	0.45 (0.43, 0.46)
600	0.43 (0.40, 0.45)
800	0.43 (0.40, 0.45)
1000	0.43 (0.41, 0.45)
Difference from $t = 40$ years	
100–40	−0.11 (-0.12, −0.10)
1000–40	−0.22 (-0.24, −0.21)
Difference from $t = 1000$ years	
1000–0	−0.40 (-0.42, −0.38)
1000–100	−0.11 (-0.13, −0.09)
1000–200	−0.05 (-0.07, −0.04)
1000–400	−0.02 (-0.03, −0.00)
1000–600	0.00 (-0.01, 0.01)
1000–800	0.00 (-0.01, 0.01)

Table 5
Summary of the tested scenarios in simulation years 100 (2072) and 600. $\langle f_u \rangle$ is the ensemble prediction of the forest fraction f_u.

Scenario	$\langle f_u \rangle$	Change from 2012
Simulation year 100		
Calibration	0.55 (0.53, 0.56)	−0.11 (-0.12, −0.10)
Decrease RI 30%	0.44 (0.43, 0.46)	−0.22 (-0.23, −0.21)
Increase severity 1x	0.50 (0.48, 0.51)	−0.17 (-0.18, −0.15)
Simulation year 600		
Calibration	0.43 (0.41, 0.46)	−0.23 (-0.25, −0.21)
Decrease RI 30%	0.20 (0.18, 0.22)	−0.46 (-0.48, −0.44)
Increase severity 1x	0.30 (0.27, 0.31)	−0.37 (-0.39, −0.34)

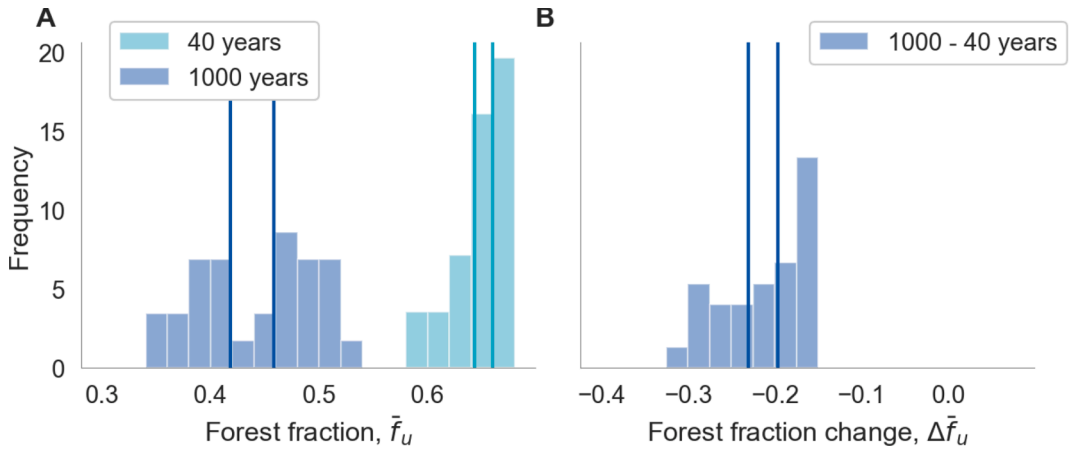

Fig. 3. (Panel A) Histograms show the calibrated ensemble prediction of the forest fraction at 40 and 1000 years. (Panel B) Histogram of the changes in forest fraction $\Delta\bar{f}_u$ between 40 and 1000 years, where Δf_u was computed separately for each parameter set. In both panels, vertical lines show the bootstrapped 95% confidence intervals for the mean. [See online article for color version of this figure.]

3.3. ICB Scenarios

Increasing fire frequency produced significant declines in forest fraction $\langle f_u \rangle$: by simulation year 100, $\langle f_u \rangle$ decreased by 22 ± 2% for a 30% decrease in *RI* (see Fig. 4A). Compared to the return interval scenario, the severity scenario resulted in a smaller but significant decline of 15 ± 2% in $\langle f_u \rangle$ by simulation year 100 (see Fig. 4B).

3.4. SCB results

Fig. 4C shows the $\langle f_u \rangle$ trajectories for the two SCB test scenarios, with the calibration simulations included for reference. The results indicate that the different return intervals between ICB and SCB are sufficient to explain the differences in $\langle f_u \rangle$ in 2012. While $\langle f_u \rangle$ was reduced by 18% between 1972 and 2012 in the ICB simulations, $\langle f_u \rangle$ decreased by only 2% in the SCB $RI \times 2.4$ simulations, highly comparable to observations suggesting a decrease on the order of 1% for the same period (Stevens et al., 2020). The prediction is not notably changed by reducing soil moisture by 10%.

3.5. Analytical results

To understand the modeled scenarios in the context of possible fire regimes, analytical response surfaces are shown in $RI - \phi$space in Fig. 5. As shown in these solutions, constant upper canopy biomass contours curve through the $RI - \phi$ space, so that upper canopy biomass is most sensitive to fire severity at moderate-high return intervals (≈ 20 years), and most sensitive to return interval at moderate-high severities (≈ 0.7), with biomass maximised at low severity and high return interval. A more complex surface emerges for the lower canopy biomass, where the peak understory biomass broadly falls along the contour for of $\widehat{G}_u \approx 5$ kg/m^2. This represents an optimum between conditions where light competition from a dense upper canopy suppresses understory growth (a situation arising for long fire return intervals and low fire severities), and conditions where fire is so frequent and severe as to suppress both upper and low canopy biomass. Unsurprisingly, the $\widehat{f}_u$ response is similar to that of $\widehat{G}_u$, although it saturates under conditions of relatively more frequent and severe fire. (See Table 6).

Points marked on Fig. 5 show the specific model scenarios tested. The analytical results demonstrate that under the managed wildfire regime, the ICB lies in a reasonably 'sensitive' part of the parameter space, where large changes in forest fraction result from modest changes in fire frequency or return interval. Conversely, the SCB is located in a 'flatter' region of the parameter space, where changes in return interval or in fire severity are unlikely to generate large changes in estimated forest fraction, even though the upper canopy biomass density may change more dramatically (panel A). Note that these surfaces treat all forest growth parameters as constant; different sensitivities to fire regime would arise if forest growth were to change in addition to fire frequency and severity. Illustrative responses to changes from calibrated parameters are shown in supporting information Fig. 4.

4. Discussion

The study investigates the long term response of forest cover to managed wildfire in two Sierra Nevada basins, its sensitivity to factors that differ between these basins, and the effects of potential climate scenarios in ICB. The model results reveal some of the value of exploratory models: despite its simplicity, the calibrated model results are consistent with the available data relating to landcover composition and responses to fire management in ICB. The model allows for synthesis of numerous observations and datasets pertaining to the fire and vegetation dynamics in the basin, and interprets their implications in terms of a variable of primary interest, the forest cover fraction. The model reveals sensitivities to different aspects of the fire regime and climate, and provides some clear indications for consideration when designing policy. This information complements detailed investigations undertaken using highly parameterized process models (Boisramé et al., 2019; Rakhmatulina et al., 2021), by allowing longer simulations and exploration of more aspects of the fire regime than have been possible for these basins to date.

The results firstly suggest that the ICB forest cover has not yet reached a stochastic steady state condition. This is consistent with the findings of Boisramé et al. (2017), who found no indication that rates of change in several landscape ecology indicators for the ICB were slowing by 2012. These model results suggest that approximately 200 years of fire suppression would be needed for the forest properties of ICB to reach stochastic steady state. This timescale is very similar to that needed for complete forest recovery following a restoration of the natural fire regime. That is - fire suppression and managed wildfire policies alter forest cover in the ICB over comparable time scales.

The time scales of forest cover response to an increase in fire frequency, however, are sensitive to the characteristics of the fire regime. As revealed by analysis of SCB, fire return intervals above a certain length may be insufficient to produce significant forest cover change in a basin, even following restoration of managed wildfire regimes. Conversely, shorter fire return intervals or increased fire severity

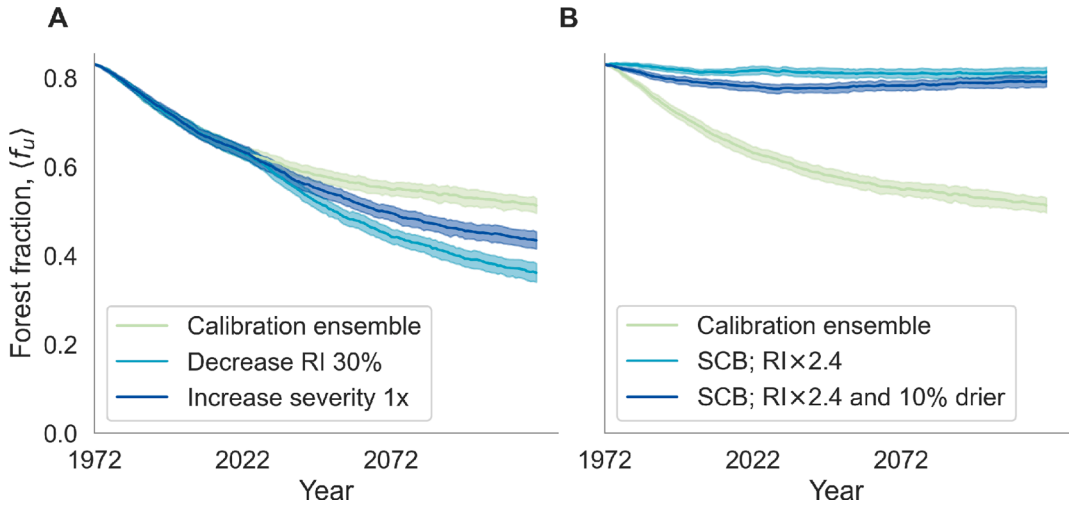

Fig. 4. Forest fraction $\langle f_u \rangle$ trajectories for (Panel A) the shorter return interval and increased severity scenarios in ICB (Panel B) the SCB test scenarios. The calibration ensemble is included for reference. [See online article for color version of this figure.]

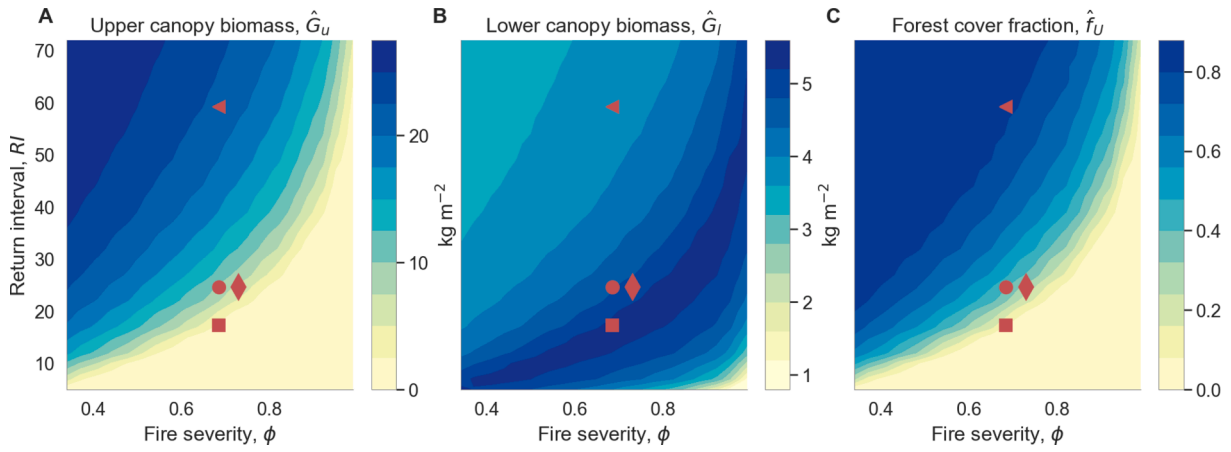

Fig. 5. Analytic predictions of the upper canopy biomass $\widehat{G}_u$ (panel A), lower canopy biomass $\widehat{G}_l$ (panel B), and forest cover fraction $\widehat{f}_u$ (panel C), as functions of fire severity ϕ and return interval *RI* (all other parameters are equal to those used to calibrate the model). Circles show the ICB observations in parameter space, squares the *RI* scenarios, diamonds the severity scenarios, and triangles the SCB *RI* scenario. [See online article for color version of this figure.]

Table 6
Summary of SCB results at 40, 100 and 600 years for two scenarios, where: (i) the return interval was increased by a factor of 2.4 in the calibrated parameter ensemble ('*RI* × 2.4'), and (ii) the soil moisture was reduced by 10% in addition to the adjusted return interval ('*RI* × 2.4 and 10% drier'). Results from the calibrated ensemble are included for reference.

Scenario	$\langle f_u \rangle$	Change from 1972
Simulation year 40		
Calibration	0.65 (0.64, 0.66)	−0.18 (-0.19, −0.17)
SCB; RI × 2.4	0.81 (0.81, 0.82)	−0.02 (-0.02, −0.01)
SCB; RI × 2.4 and 10% drier	0.79 (0.78, 0.79)	−0.04 (-0.05, −0.04)
Simulation year 100		
Calibration	0.54 (0.53, 0.55)	−0.29 (-0.30, −0.28)
SCB; RI × 2.4	0.81 (0.80, 0.82)	−0.02 (-0.03, −0.01)
SCB; RI × 2.4 and 10% drier	0.78 (0.77, 0.79)	−0.05 (-0.06, −0.04)
Simulation year 600		
Calibration	0.43 (0.41, 0.45)	−0.40 (-0.42, −0.38)
SCB; RI × 2.4	0.82 (0.80, 0.83)	−0.01 (-0.03, 0.00)
SCB; RI × 2.4 and 10% drier	0.82 (0.80, 0.83)	−0.01 (-0.03, −0.00)

accelerate the rate of forest cover conversion (Coop et al., 2020; Stephens et al., 2021). These changes do not necessarily represent a viable management approach, however, as the rapid rate of forest conversion is also associated with lower steady state forest cover. For example, a 30% reduction in fire return interval in ICB imposed in 2022 results in the forest cover approaching a value similar to the 'natural' steady state over a 50 year timeframe (Fig. 4A). However, in the long term (600 years), such a frequent fire regime results in a very low stationary forest cover of 0.2 in the basin.

The simulations suggest that the distinction between ICB and SCB forest cover trajectories is explained by the difference in fire regime between the two basins. The simple model cannot, however, determine why the fire return intervals are so distinct between the two basins. There is a known management component associated with the use of fire suppression in SCB, but it is not clear if the different fire regimes in the basins are completely, or only partly attributable to these management differences.

The modeled forest cover was very sensitive to the difference in fire return interval between the basins. As revealed by the analytical results, the steady state conditions are most sensitive to return interval for intermediate values of fire severity ($\widehat{\phi}_u \approx 0.7$), with less sensitivity to return interval when fire severity is very high or low. Similarly, the results are most sensitivity to fire severity for intermediate return intervals (*RI* ≈ 20 years). Consequently, where both return interval and severity adopt moderate values, the outcomes for forest cover are likely to be sensitive to changes in fire conditions. Furthermore, as shown in the analytical results presented in the supporting information, and made clear in the expressions Eq. 10 and 13, forest cover is also influenced by growth rates.

While predicting the long-term forest cover is difficult, the findings suggest cautious optimism in applying the managed wildfire approach to new basins. Decreasing fire return intervals within fire suppressed forests appear to be likely to produce long-term changes in forest cover. Where fire return intervals are lengthy, the simplest management tool is to increase the fire frequency. If this can be achieved while managing the initial risk of extensive high severity fire, there is every reason to expect forest cover to be reduced without severely impacting the local ecology and ecosystem services in the process - an outcome which itself reduces the risk of extensive high severity fire long-term. While the outcomes of managed wildfire remain uncertain, the model results suggest that targeting a reduction in fire return intervals is a viable pathway for reversing the effects of fire suppression.

The results suggest that changes in fire regime associated with a changing climate have the potential to alter the outcomes of a managed wildfire policy. To date, increases in fire severity within the managed basins have been negligible, and even projecting forward the changes in fire severity experienced across the broader Sierra Nevada shows comparable influence on forest cover to the differences in return interval between the basins. Most changes expected under a changing climate would tend to reduce forest cover in the managed wildfire basins.

However, despite the appeal and simplicity of the exploratory model, these 'extrapolated' results must be interpreted within the limitations of the simple model structure and parameterization. Several processes that could importantly influence vegetation cover trajectories, including feedbacks between vegetation biomass and soil moisture, competition between canopy layers suppressing the upper canopies species, and the relationships between vegetation biomass and the fire characteristics of the landscape, are all omitted from the model.

Future trends in fire severity will be determined by a number of interacting factors, which are not included in the simple model framework presented here. For example, increasingly frequent and hotter droughts are expected to result in increasingly flammable fuel conditions (Brando et al., 2014) and heavy downed woody fuels from drought and bark beetle tree mortality can lead to increased fire severity (Stephens et al., 2018; Stephens et al., 2022). Alternatively, increasing levels of drought-related tree mortality may reduce risks of high-severity stand-replacing fire by reducing ladder fuels (Hicke et al., 2012) and canopy fuels (Stephens et al., 2018). Predicting how these factors will play out in the Illilouette and Sugarloaf Creek Basins is challenging, and was not attempted here.

The role of CO_2 was similarly omitted from the long-term predictions (Topic 1) and fire regime scenarios (Topic 2) estimating forest cover changes over time. Global atmospheric CO_2 levels have increased since managed wildfire regimes were implemented and will continue to increase. Increasing CO_2 influences vegetation growth (Ma et al., 2015; Saha et al., 2015), and interacts with other climate effects (e.g., drought stress, Duan et al., 2018) and edaphic conditions, favoring the growth of some species over others under future conditions (Niinemets et al., 2011). The projected long-term response of the ICB to the managed wildfire regime does not consider variable growth rates in response to rising CO_2, nor how higher CO_2 and associated changes in hydroclimate (e.g., increasing drought severity) will interact to change vegetation growth rates.

These omissions mean that the model is most appropriately used within the context of its calibration, i.e., for forest cover in the range 0.65–0.83. Results that extrapolate outside this range – and several of the results are based on such extrapolations – are necessarily speculative. For example, as forest cover declines, the rate and extent of fire spread through ICB may change, relative to the 0.65–0.83 forest fraction case. Since spatial fire spread is not represented in the model, its effects on forest cover dynamics is accounted for using the calibrated return interval and forest growth parameters. The stationarity of these parameters across the simulated range of forest cover is not known - but it would be expected, for instance, that when forest cover becomes very sparse (Parks et al., 2015), fires might be spatially constrained by fuel limitations, as is known to already occur in ICB (Collins et al., 2009; Collins et al., 2016). Thus, the more extreme scenarios in which forest cover approaches zero may be exaggerated due to spatial constraints omitted from the model. Similarly, the stability of high forest cover across the parameter space (e.g. the large blue areas on Fig. 5C) may be exaggerated, as the probability of fires spreading rapidly across large areas is not well captured when calibrating to the fragmented ICB landscape. Consequently, the results are most reasonably interpreted when considering small shifts in forest and fire properties relative to ICB.

The results suggest that, at present, the ICB has not yet reached a stochastic steady state, and that its forest cover will likely continue to decline if the managed wildfire regime continues. They suggest that forest change through manipulation of fire regimes is a slow and variable process, with a final outcome likely to be influenced by ongoing changes in forest growth rates and fire regime properties. They suggest that insufficient decrease in fire return interval compared to suppressed conditions may result in little observable change in forests from today's conditions. Managed wildfire remains an appealing instrument for forest restoration – but one which is likely to need ongoing monitoring and research to fully understand and shape its impacts on the landscape.

Declaration of Competing Interest

The authors declare that they have no known competing financial interests or personal relationships that could have appeared to influence the work reported in this paper.

Acknowledgments

OC, SET, and ER acknowledge funding from National Science Foundation EAR Grant 1013339. GB acknowledges funding from National Science Foundation CZCN Grant 2011346. We thank Anneliese Sytsma and Jean Wilkening for their comments and suggestions on the manuscript, and Brandon Collins and Jens Stevens for their helpful feedback on the project concept. We thank Jan van Wagtendonk for introducing us to the ICB and for his inspiration to work there.

Data used to calibrate the model, and model code to run a sample simulation are available through the Center for Open Science at: https://osf.io/x2yzj.

Vegetation maps for Illilouette Creek Basin can be downloaded from: https://doi.org/10.1016/j.foreco.2017.07.034

Appendix A. Supplementary material

Supplementary data associated with this article can be found, in the online version, at https://doi.org/10.1016/j.foreco.2022.120429.

References

Abatzoglou, J.T., Williams, A.P., Boschetti, L., Zubkova, M., Kolden, C.A., 2018. Global patterns of interannual climate–fire relationships. Global Change Biol. 24 (11), 5164–5175.

Allen, C.D., Breshears, D.D., McDowell, N.G., 2015. On underestimation of global vulnerability to tree mortality and forest die-off from hotter drought in the anthropocene. Ecosphere 6 (8), 1–55.

Boisramé, G., Thompson, S., Collins, B., Stephens, S., 2017. Managed wildfire effects on forest resilience and water in the sierra nevada. Ecosystems 20 (4), 717–732.

Boisramé, G., Thompson, S., Stephens, S., 2018. Hydrologic responses to restored wildfire regimes revealed by soil moisture-vegetation relationships. Adv. Water Resour. 112, 124–146.

Boisramé, G., Thompson, S.E., Kelly, M., Cavalli, J., Wilkin, K.M., Stephens, S., 2017. Vegetation change during 40 years of repeated managed wildfires in the Sierra Nevada, California. For. Ecol. Manage. 402, 241–252.

Boisramé, G.F., Thompson, S.E., Tague, C., Stephens, S.L., 2019. Restoring a natural fire regime alters the water balance of a Sierra Nevada catchment. Water Resour. Res. 55 (7), 5751–5769.

Boisrameé, G., Brown, T., & Bachelet, D. (2022). Trends in western US fire fuels using historical data and modeling. Fire Ecology, In press.

Bradstock, R.A., Hammill, K.A., Collins, L., Price, O., 2010. Effects of weather, fuel and terrain on fire severity in topographically diverse landscapes of south-eastern australia. Landscape Ecol. 25 (4), 607–619.

Brando, P.M., Balch, J.K., Nepstad, D.C., Morton, D.C., Putz, F.E., Coe, M.T., et al., 2014. Abrupt increases in amazonian tree mortality due to drought–fire interactions. Proc. Nat. Acad. Sci. 111 (17), 6347–6352.

Bullock, S. (1982). Reproductive ecology of ceanothus cordulatus, (Unpublished master's thesis). California State University, Fresno.

Butler, B.W., Dickinson, M.B., 2010. Tree injury and mortality in fires: developing process-based models. Fire Ecology 6 (1), 55–79.

Casagrandi, R., Rinaldi, S., 1999. A minimal model for forest fire regimes. Am. Nat. 153 (5), 527–539.

Coen, J.L., Schroeder, W., Conway, S., Tarnay, L., 2020. Computational modeling of extreme wildland fire events: a synthesis of scientific understanding with applications to forecasting, land management, and firefighter safety. Journal of Computational Science 101152.

Collins, B.M., Everett, R.G., Stephens, S.L., 2011. Impacts of fire exclusion and recent managed fire on forest structure in old growth sierra nevada mixed-conifer forests. Ecosphere 2 (4), 1–14.

Collins, B.M., Lydersen, J.M., Fry, D.L., Wilkin, K., Moody, T., Stephens, S.L., 2016. Variability in vegetation and surface fuels across mixed-conifer-dominated landscapes with over 40 years of natural fire. For. Ecol. Manage. 381, 74–83.

Collins, B.M., Miller, J.D., Thode, A.E., Kelly, M., Van Wagtendonk, J.W., Stephens, S.L., 2009. Interactions among wildland fires in a long-established sierra nevada natural fire area. Ecosystems 12 (1), 114–128.

Collins, B.M., Stephens, S.L., 2007. Managing natural wildfires in sierra nevada wilderness areas. Front. Ecol. Environ. 5 (10), 523–527.

Coop, J.D., Parks, S.A., Stevens-Rumann, C.S., Crausbay, S.D., Higuera, P.E., Hurteau, M. D., et al., 2020. Wildfire-driven forest conversion in western north american landscapes. Bioscience 70 (8), 659–673.

Dillon, G.K., Holden, Z.A., Morgan, P., Crimmins, M.A., Heyerdahl, E.K., Luce, C.H., 2011. Both topography and climate affected forest and woodland burn severity in two regions of the western us, 1984 to 2006. Ecosphere 2 (12), 1–33.

D'Odorico, P., Laio, F., Ridolfi, L., 2006. A probabilistic analysis of fire-induced tree-grass coexistence in savannas. Am. Nat. 167 (3), E79–E87.

Donohue, R.J., Roderick, M.L., McVicar, T.R., Farquhar, G.D., 2013. Impact of co2 fertilization on maximum foliage cover across the globe's warm, arid environments. Geophys. Res. Lett. 40 (12), 3031–3035.

Duan, H., Huang, G., Zhou, S., Tissue, D.T., 2018. Dry mass production, allocation patterns and water use efficiency of two conifers with different water use strategies under elevated [co2], warming and drought conditions. Eur. J. Forest Res. 137 (5), 605–618.

Favier, C., Chave, J., Fabing, A., Schwartz, D., Dubois, M.A., 2004. Modelling forest–savanna mosaic dynamics in man-influenced environments: effects of fire, climate and soil heterogeneity. Ecological modelling 171 (1–2), 85–102.

Gonzalez, P., Battles, J.J., Collins, B.M., Robards, T., Saah, D.S., 2015. Aboveground live carbon stock changes of california wildland ecosystems, 2001–2010. For. Ecol. Manage. 348, 68–77.

Hicke, J.A., Johnson, M.C., Hayes, J.L., Preisler, H.K., 2012. Effects of bark beetle-caused tree mortality on wildfire. For. Ecol. Manage. 271, 81–90.

Hoffmann, W.A., Bazzaz, F.A., Chatterton, N.J., Harrison, P.A., Jackson, R.B., 2000. Elevated co2 enhances resprouting of a tropical savanna tree. Oecologia 123 (3), 312–317.

Huff, S., Poudel, K.P., Ritchie, M., Temesgen, H., 2018. Quantifying aboveground biomass for common shrubs in northeastern california using nonlinear mixed effect models. Forest ecology and management 424, 154–163.

Kane, V.R., North, M.P., Lutz, J.A., Churchill, D.J., Roberts, S.L., Smith, D.F.,... Brooks, M.L. (2014). Assessing fire effects on forest spatial structure using a fusion of landsat

and airborne lidar data in yosemite national park. Remote Sensing of Environment 151, 89–101.
Larsen, L., Thomas, C., Eppinga, M., Coulthard, T., 2014. Exploratory modeling: Extracting causality from complexity. Eos, Transactions American Geophysical Union 95 (32), 285–286.
Larsen, L.G., Eppinga, M.B., Passalacqua, P., Getz, W.M., Rose, K.A., Liang, M., 2016. Appropriate complexity landscape modeling. Earth-science reviews 160, 111–130.
Leopold, A.S. (1963). Wildlife management in the national parks. US National Park Service.
Li, C., Corns, I.G., Yang, R.C., 1999. Fire frequency and size distribution under natural conditions: a new hypothesis. Landscape Ecol. 14 (6), 533–542.
Loudermilk, E.L., Scheller, R.M., Weisberg, P.J., Yang, J., Dilts, T.E., Karam, S.L., Skinner, C., 2013. Carbon dynamics in the future forest: the importance of long-term successional legacy and climate–fire interactions. Global change biology 19 (11), 3502–3515.
Ma, X., Huete, A., Moran, S., Ponce-Campos, G., Eamus, D., 2015. Abrupt shifts in phenology and vegetation productivity under climate extremes. Journal of Geophysical Research: Biogeosciences 120 (10), 2036–2052.
Mackey, B., Lindenmayer, D., Norman, P., Taylor, C., Gould, S., 2021. Are fire refugia less predictable due to climate change? Environ. Res. Lett. 16 (11), 114028.
Mann, M.L., Batllori, E., Moritz, M.A., Waller, E.K., Berck, P., Flint, A.L.,... Dolfi, E. (2016). Incorporating anthropogenic influences into fire probability models: Effects of human activity and climate change on fire activity in california. PLoS One 11(4), e0153589.
Maxwell, C., Scheller, R., 2020. Identifying habitat holdouts for high elevation tree species under climate change. front. for. glob. Change 2, 94.
Miller, C., Urban, D.L., 1999. Forest pattern, fire, and climatic change in the sierra nevada. Ecosystems 2 (1), 76–87.
Miller, J.D., Collins, B.M., Lutz, J.A., Stephens, S.L., van Wagtendonk, J.W., Yasuda, D.A., 2012. Differences in wildfires among ecoregions and land management agencies in the sierra nevada region, california, usa. Ecosphere 3 (9), 1–20.
Miller, J.D., Thode, A.E., 2007. Quantifying burn severity in a heterogeneous landscape with a relative version of the delta normalized burn ratio (dnbr). Remote Sens. Environ. 109 (1), 66–80.
Niinemets, Ü., Flexas, J., Peñuelas, J., 2011. Evergreens favored by higher responsiveness to increased co2. Trends in Ecology & Evolution 26 (3), 136–142.
North, M., Collins, B.M., Stephens, S., 2012. Using fire to increase the scale, benefits, and future maintenance of fuels treatments. J. Forest. 110 (7), 392–401.
Parks, S.A., Holsinger, L.M., Miller, C., Nelson, C.R., 2015. Wildland fire as a self-regulating mechanism: the role of previous burns and weather in limiting fire progression. Ecol. Appl. 25 (6), 1478–1492.
Parks, S.A., Holsinger, L.M., Voss, M.A., Loehman, R.A., Robinson, N.P., 2018. Mean composite fire severity metrics computed with google earth engine offer improved accuracy and expanded mapping potential. Remote Sensing 10 (6), 879.
Parsons, D.J., 1976. The role of fire in natural communities: an example from the southern sierra nevada, california. Environ. Conserv. 3 (2), 91–99.
Ponisio, L.C., Wilkin, K., M'Gonigle, L.K., Kulhanek, K., Cook, L., Thorp, R.,... Kremen, C. (2016). Pyrodiversity begets plant–pollinator community diversity. Global change biology 22(5), 1794–1808.
Rakhmatulina, E., Boisramé, G., Stephens, S.L., Thompson, S., 2021. Hydrological benefits of restoring wildfire regimes in the sierra nevada persist in a warming climate. J. Hydrol. 593, 125808.
Rakhmatulina, E., Stephens, S., Thompson, S., 2021. Soil moisture influences on sierra nevada dead fuel moisture content and fire risks. For. Ecol. Manage. 496, 119379.
Rastetter, E.B., 2017. Modeling for understanding v. modeling for numbers. Ecosystems 20 (2), 215–221.
Rothman, H.K., 2007. Blazing heritage: a history of wildland fire in the national parks. Oxford University Press on Demand.
Saha, M., Scanlon, T., D'odorico, P., 2015. Examining the linkage between shrub encroachment and recent greening in water-limited southern africa. Ecosphere 6 (9), 1–16.
Seidl, R., Fernandes, P.M., Fonseca, T.F., Gillet, F., Jönsson, A.M., Merganičová, K., et al., 2011. Modelling natural disturbances in forest ecosystems: a review. Ecol. Model. 222 (4), 903–924.
Stephens, S., Bernal, A., Collins, B., Finney, M., Lautenberger, C., Saah, D., 2022. Mass fire behavior created by extensive tree mortality and high density not predicted by operational fire behavior models in the southern sierra nevada. For. Ecol. Manage. In press.
Stephens, S., Collins, B.M., Fettig, C.J., Finney, M.A., Hoffman, C.M., Knapp, E.E.,... Wayman, R.B. (2018). Drought, tree mortality, and wildfire in forests adapted to frequent fire. BioScience 68(2), 77–88.
Stephens, S., Martin, R.E., Clinton, N.E., 2007. Prehistoric fire area and emissions from california's forests, woodlands, shrublands, and grasslands. For. Ecol. Manage. 251 (3), 205–216.
Stephens, S., Thompson, S.E., Boisrame, G., Collins, B.M., Ponisio, L., Rakhmatulina, E.,... Wilken, K. (2021). Fire, water, and biodiversity in the Sierra Nevada: A possible triple win. Environmental Research Communications 3(8).
Stephens, S., Westerling, A.L., Hurteau, M.D., Peery, M.Z., Schultz, C.A., Thompson, S., 2020. Fire and climate change: Conserving seasonally dry forests is still possible. Front. Ecol. Environ. 18 (6), 354–360.
Stevens, J.T., Boisramé, G.F., Rakhmatulina, E., Thompson, S.E., Collins, B.M., Stephens, S.L., 2020. Forest vegetation change and its impacts on soil water following 47 years of managed wildfire. Ecosystems 1–19.
Taylor, A.H., Skinner, C.N., 1998. Fire history and landscape dynamics in a late-successional reserve, klamath mountains, california, usa. For. Ecol. Manage. 111 (2–3), 285–301.
Taylor, A.H., Trouet, V., Skinner, C.N., Stephens, S., 2016. Socioecological transitions trigger fire regime shifts and modulate fire–climate interactions in the Sierra Nevada, USA, 1600–2015 ce. Proc. Nat. Acad. Sci. 113 (48), 13684–13689.
Ursino, N., Rulli, M.C., 2011. Hydrological minimal model for fire regime assessment in a mediterranean ecosystem. Water Resour. Res. 47 (11).
Wayman, R.B., Safford, H.D., 2021. Recent bark beetle outbreaks influence wildfire severity in mixed-conifer forests of the sierra nevada, california, usa. Ecol. Appl. 31 (3), e02287.
Westerling, A.L. (2018). Wildfire simulations for california's fourth climate change assessment: Projecting changes in extreme wildfire events with a warming climate: a report for california's fourth climate change assessment. California Energy Commission Sacramento, CA.
Westerling, A.L., Bryant, B., 2008. Climate change and wildfire in california. Climatic Change 87 (1), 231–249.
Wilkening, J.V., Cardillo, E., Abad, E., Thompson, S.E., 2021. Saturation excess overland flow accelerates the spread of a generalist soil-borne pathogen. J. Hydrol. 593, 125821.
Yue, X., Mickley, L.J., Logan, J.A., 2014. Projection of wildfire activity in southern california in the mid-twenty-first century. Climate dynamics 43 (7), 1973–1991.
Zhu, Z., Piao, S., Myneni, R.B., Huang, M., Zeng, Z., Canadell, J.G., et al., 2016. Greening of the earth and its drivers. Nat. Clim. Change 6 (8), 791–795.